Bursting dynamics of a fiber laser with an injected signal

David J. DeShazer,[1] J. García-Ojalvo,[2] and Rajarshi Roy[1,*]
[1]*Department of Physics and Institute for Research in Electronics and Applied Physics, University of Maryland, College Park, Maryland 20742*
[2]*Departament de Física i Enginyeria Nuclear, Universitat Politècnica de Catalunya, Colom 11, E–08222 Terrassa, Spain*
(Received 21 October 2002; published 11 March 2003)

We study the effect of near-resonant optical injection on the dynamical behavior of an erbium-doped fiber ring laser. Our experimental results show that, in the presence of even a small amount of injection, the output laser intensity exhibits bursts spaced irregularly in time and with randomly varying amplitudes. A heterodyne measurement of the frequency dynamics of the laser suggests that this bursting is due to an irregular wandering of the laser frequency through the injection locking range. This interpretation is confirmed by a systematic analysis of a simplified rate-equation model in which the frequency wandering is modeled phenomenologically by means of a temporally correlated noise. A statistical analysis of the bursting events is performed, displaying satisfactory agreement between the experiment and the model. In particular, the interburst time distribution exhibits a well defined power law decay over a sizable time range.

DOI: 10.1103/PhysRevE.67.036602 PACS number(s): 42.65.Sf, 42.60.Mi, 05.45.−a, 05.40.−a

I. INTRODUCTION

Bursting is a common feature in many natural systems, arising in fields such diverse as hydrodynamic turbulence [1], binary fluid convection [2], plasma confinement [4], magnetohydrodynamics [3], x-ray pulsar emission [5], and neural processing [6]. Bursting events are typically characterized by sudden, short-lived, high-amplitude deviations of a nonlinear dynamical system from its otherwise quiescent state (although in the neuroscience literature these events are called spikes, the term ''burst'' being reserved for repetitive spiking). Due to its ubiquity and conspicuity, understanding the different mechanisms that give rise to bursting is a topic of significant current interest. Optical systems, and in particular lasers, are exceptionally suited for that purpose, due to their experimental controllability and the deep understanding of the physical mechanisms underlying their dynamical operation attained over the years [7]. By way of example, neural-like bursting behavior associated with homoclinic chaos has been recently observed in a CO_2 laser with feedback-modulated losses [8]. In the present paper, we report on the bursting behavior exhibited by an optical fiber laser under the influence of weak optical injection, and elucidate the mechanism leading to this behavior.

Injection locking of lasers [9] is a standard technique used for a wide range of technological applications, including power amplification and stabilization [10], polarization control [11], and frequency stabilization [12,13]. Injection locking has also been successfully used recently to enhance coherence in broad-area lasers [14] and laser arrays [15]. But besides its technological applications, optical injection is also known to induce complex dynamical behavior in lasers [16]. Special attention has been recently paid to the case of semiconductor lasers, for which the injection-locked state is unstable for most parameter values [17], leading to a very rich bifurcation structure [18]. A similar scenario exists in solid-state lasers [19], although in that case the stationary locked state is stable over a larger region of parameter space [20], provided the detuning between the injected and the laser frequencies is small. In the opposite limit of large detunings, the injected beam has basically no effect on the laser field and the dynamics is again approximately stationary. Still, for intermediate values of the frequency detuning (around the limits of the locking range) the system exhibits complex dynamical oscillations [21]. Under these conditions, one can already envisage that if the laser would autonomously wander into and out of the locking range, the emitted intensity would exhibit bursts as the system crossed the locking region. As we will show below, both experimentally and with the help of a phenomenologically oriented rate-equation model, this is the mechanism leading to bursts in injected optical-fiber lasers.

Optical-fiber lasers are a type of solid-state laser whose amplifying medium is an optical fiber doped with rare-earth atoms. Due to their usually very long cavities, fiber lasers have a large number of closely spaced longitudinal modes, packed within a very broad gain line produced by the inhomogeneous broadening of the amorphous host medium. This implies that these lasers usually operate in a large number of modes. In spite of this fact, fiber lasers have attracted great technological interest in recent years. In particular, erbium-doped fiber lasers have an emission wavelength that precisely matches the spectral range of minimal absorption in standard silica optical fibers. For that reason, erbium-doped fiber amplifiers have become standard elements in optical communication systems [22]. Recently, interest has arised in the development of fiber laser arrays operating in a phase-locked state via evanescent wave coupling [23]. Here, we examine optical injection of a steady coherent beam into a fiber laser. This situation is relevant for communication applications in which the fiber laser itself plays the role of a receptor [24]. In what follows, we show that due to the complex dynamical behavior of fiber lasers, even a small amount of injection induces intense bursting in the system.

*Also at the Institute for Physical Science and Technology, University of Maryland, College Park, MD 20742.

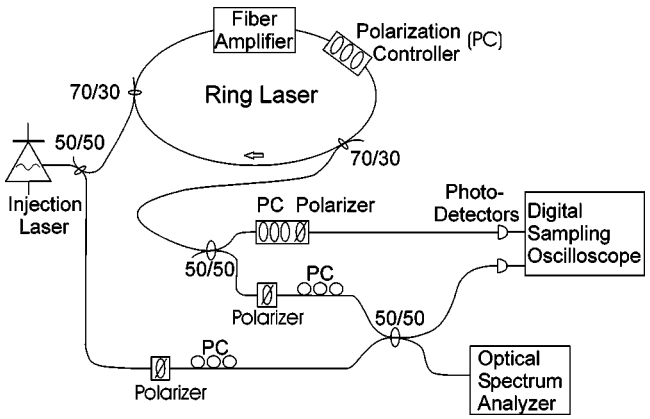

FIG. 1. Experimental setup: an erbium-doped fiber ring laser (top) is subject to optical injection from an external-cavity semiconductor laser (left). Part of the light emitted by this laser is used as a reference beam in a heterodyne measurement performed at the 50-50 coupler at the bottom of the figure.

II. EXPERIMENTAL STUDY

Figure 1 shows the experimental setup used in what follows. The laser consists of a ring of optical fiber with a total length of 41.5 m. The active element of the fiber ring is an erbium-doped fiber amplifier containing 17 m of doped fiber, a 980-nm semiconductor pumping laser, and a Faraday optical isolator that enforces unidirectional light propagation inside the ring. All passive and active fiber is single mode, nonpolarization maintaining. An optical waveplate polarization controller allows tuning of the net birefringence of the fiber ring, and hence its lasing frequency, among other characteristics. We select a mode of operation where the laser displays a single-peaked spectrum centered at $\lambda_L = 1557.8$ nm, with a full width at half maximum (FWHM) of $\Delta\lambda_L \sim 0.6$ nm ($\Delta\nu_L \sim 74$ GHz). Light from the ring laser is extracted with a 70-30 coupler, and its dynamics is analyzed by measuring its intensity with a 125-MHz bandwidth photodetector and a 1-GHz bandwidth digital sampling oscilloscope. The ring laser is operated far above threshold, at a pump power of 130 mW, with the lasing threshold located at about 10 mW. Under these conditions the optical power circulating in the ring is $P_L \approx 9$ mW.

Bursting is induced in the erbium-doped fiber ring laser by monochromatic injection from an external-cavity semiconductor laser. The injected signal, with constant intensity, is introduced into the ring cavity using a 70-30 fiber-optic evanescent field coupler. The injection laser is tuned to match the peak wavelength of the fiber laser, i.e., $\lambda_{\mathrm{inj}} = 1557.8$ nm, while its spectrum exhibits a FWHM of $\Delta\lambda_{\mathrm{inj}} \sim 1.2$ fm ($\Delta\nu_{\mathrm{inj}} \sim 150$ kHz), much smaller than that of the ring laser. The difference in the spectral widths of the two lasers highlights the fact that the injection laser operates in a single longitudinal mode, whereas the fiber ring laser is highly multimode: given that the ring length is $L = 41.5$ m, consecutive longitudinal modes in the fiber laser are separated by a free spectral range $\Delta\nu_{\mathrm{sp}} = c/(nL) = 5$ MHz, where c is the speed of light in vacuum and $n = 1.444$ is the index of refraction of fused silica. Since the spectral width of the fiber laser is $\Delta\nu_L \sim 74$ GHz, one can conclude that thousands of modes are active in this laser.

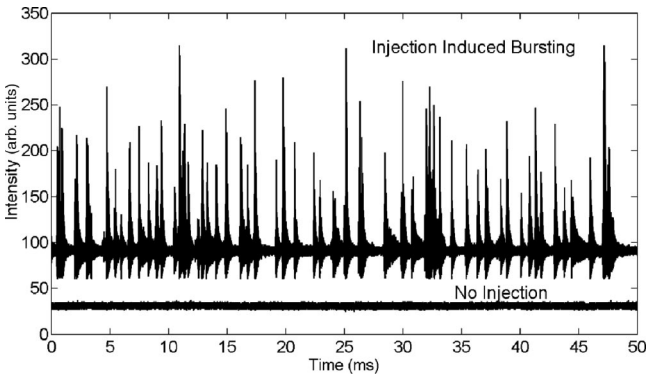

FIG. 2. Temporal evolution of the light intensity emitted by the erbium-doped fiber ring laser with (top) and without (bottom) injection. The top time trace has been shifted upwards for clarity.

The intensity time traces of the light emitted by the fiber ring laser with and without injection are compared in Fig. 2. In the absence of injection (bottom trace), the laser operates in a stationary regime exhibiting a non-negligible but constant amount of fast fluctuations (indiscernible in the figure) caused by its complex multimode operation. When a small amount of light (in this case the power ratio is $P_{\mathrm{inj}}/P_L = 2.8\times10^{-3}$) is injected into the cavity (top trace, shifted upwards in the figure for clarity), the laser exhibits intense bursts with nonconstant amplitudes and at irregular times. These bursts are not single-spike events, but are followed by decaying oscillations [see Fig. 4(a)] towards the base level, where the system remains until the next burst. These decaying oscillations occur at a frequency approximately equal to the relaxation oscillation frequency of the free-running laser, $\nu_{\mathrm{RO}} \sim 45$ kHz for the pump power used, which is much higher than the typical bursting frequency.

The bursting behavior shown in Fig. 2 was obtained by tuning the injected wavelength to resonance with the lasing wavelength (within experimental precision). However, the same qualitative behavior persists for a wide range of injected wavelengths, with the mean burst amplitude decreasing and the interburst time separation increasing as the detuning increases, until for $\Delta\lambda \sim 14$ nm all bursts have disappeared and the intensity dynamics becomes nearly identical to a ring laser without injection (bottom plot). We believe that this extremely large bursting range is due to the broad width of the optical gain of erbium-doped fiber [25].

III. FREQUENCY DYNAMICS OF THE FIBER LASER

The results presented above do not exhibit the qualitative characteristics usually displayed by injected lasers. Normally, an injected solid-state laser would operate in a stable locked state for low enough detuning between the injected and free-running laser frequencies. For very large detunings, the injection would have no effect and the laser would behave as in the free-running stationary regime. For intermediate detunings, well-defined periodic or chaotic dynamics would arise [19,21], all of them qualitatively different from

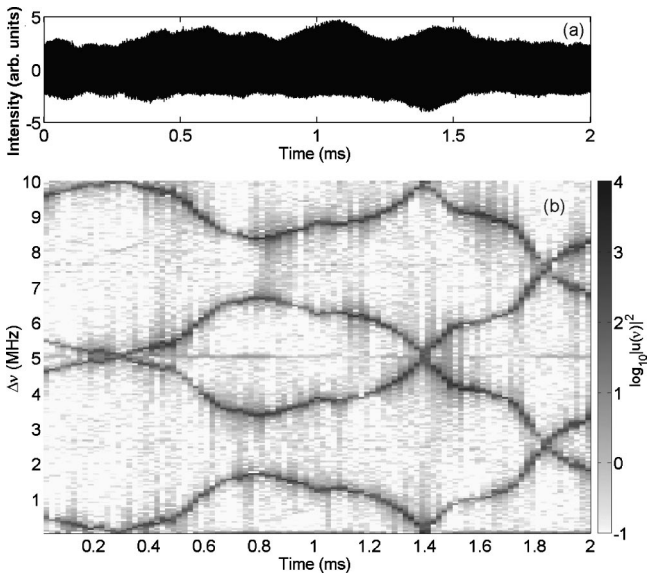

FIG. 3. Longitudinal mode structure of the fiber ring laser without injection: ring laser intensity dynamics (a) and its corresponding spectrogram, with the detuning with respect to the reference injection frequency plotted in the vertical axis (b). The intensity axis in (a) has been rescaled to zero mean and normalized to the standard deviation of the original time series. Sampling rate was 5×10^8 s^{-1}.

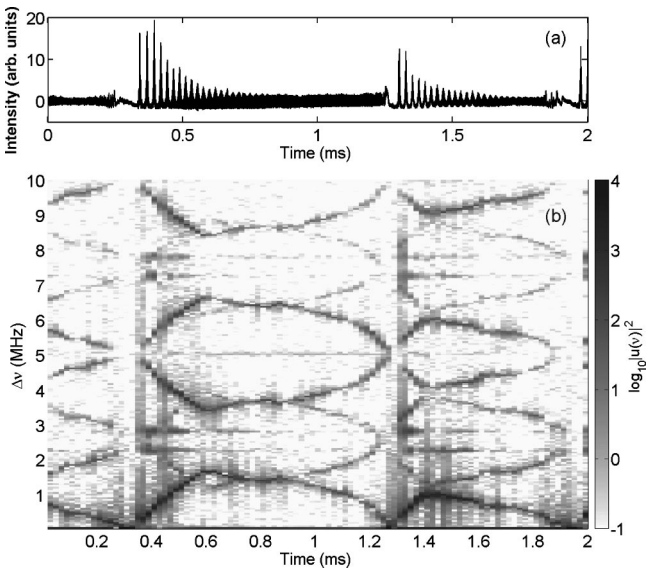

FIG. 4. Longitudinal mode structure of the fiber ring laser with injection: ring laser intensity dynamics (a) and its corresponding spectrogram (b), plotted as in Fig. 3. The injected power ratio is $P_{\mathrm{inj}}/P_L = 7.4 \times 10^{-2}$. The faint ghost images forming additional sets of modes are due to orthogonally polarized light projected on the linear polarization state sampled by the polarizers in the fiber-laser heterodyne channel.

the bursting state described above. In order to reconcile the present results with our previous understanding of injected lasers, we need to determine the detuning regime in which our laser is operating. In this sense, we note that most previous studies in this field have concentrated on single mode (or weakly multimode) lasers, whereas the fiber laser being investigated here is strongly multimode. As we will show, this fact has important consequences on the system behavior, particularly in its frequency dynamics, even in the absence of injection.

With the aim of studying the dynamical behavior of the lasing frequency, we conduct a simple heterodyne experiment using the setup plotted in Fig. 1. The external-cavity injection laser provides an ideal, stable reference laser for the heterodyne experiment due to its good frequency stability (optical frequency fluctuations are smaller than tens of kHz). A 50-50 coupler diverts one half of the injection-laser output to a reference channel. The fiber-laser output is also split into two equal parts using another 50-50 coupler. Half of the ring laser output is detected directly by the photodetector and the digital oscilloscope, while the other half is combined with the reference beam at a third 50-50 coupler. All fiber lengths in the experimental setup are matched for simultaneous detection. Furthermore, the polarization states of the fiber and reference laser beams are matched using both polarization controllers and linear polarizers before being combined in the heterodyne channel.

Since the fiber laser output consists of many hundreds of lasing modes, the combined beam exhibits intensity fluctuations that correspond to a superposition of the beatings between each of these modes and the stable reference frequency of the external cavity laser. The beat dynamics is isolated by subtracting the pure fiber laser intensity time series from the combined signal. A time-resolved spectral analysis of the resulting time series, making use of Fourier transforms of 20-μs segments with no overlap, gives rise to the spectrogram shown in Fig. 3(b). This figure shows the frequency dynamics of the longitudinal modes closer to the reference (i.e., injected) frequency, which corresponds to the intensity evolution shown in Fig. 3(a). The longitudinal modes of the free running laser, separated by the free spectral range $\nu_{\mathrm{sp}} = 5$ MHz, are represented by each of the wandering dark gray trajectories shown in the spectrogram. Note that within a detuning range of 5 MHz, there are two modes whose wanderings seem to mirror each other. This is due to the fact that the frequency of the intensity fluctuations in the combined heterodyne signal gives the absolute value of the detuning between the fiber laser modes and the reference laser. Therefore, a negatively detuned mode is folded over to a positive detuning in the spectrogram, and appears as a mirror image of the symmetric positively detuned mode. This produces spurious reflections of the wandering mode off the zero-detuning reference axis [like the one at 1.4 ms in Fig. 3(b)] which actually correspond to crossings of the mode through the reference frequency, followed by a shifting from positive to negative detuning, or vice versa.

In any case, once all such artifacts are accounted for in Fig. 3(b), the remarkable conclusion that one can draw from this figure is that the longitudinal modes of the fiber laser wander over a range of several megahertz, in an apparently random way, maintaining their constant 5-MHz frequency spacing, at a time scale on the order of milliseconds, much slower than the typical time scale of the intensity fluctuations [see Fig. 3(a)]. The origin of this slow frequency wandering

(which, we remark, occurs in the absence of injection) is still an open question, although qualitative considerations lead us to think that it is due to the complex interaction between the many modes operating in the laser [26].

We now perform the heterodyne measurement in the presence of injection. The result is shown in Fig. 4 for two consecutive bursting events. At the temporal resolution of this measurement, the relaxation oscillations following each burst can be clearly identified [Fig. 4(a)]. The corresponding spectrogram shows that, while the slow frequency wandering persists in the presence of injection, the bursting events are clearly associated with instantaneous locking of the fiber laser to the injected signal. Locking occurs when one of the wandering modes comes close enough to the injection frequency. At this point, this locked mode absorbs all the lasing power, and all the other modes of the ring laser vanish, rendering the laser momentarily single mode. Locking is evident in the intensity time series [Fig. 4(a)] as a sharp decrease in the amplitude of intensity fluctuations. The system does not remain locked for long, and the laser leaves the locking regime abruptly, accompanied by an intensity burst. The total intensity performs relaxation oscillations towards its initial preburst state, which is similar to that of the free-running fiber laser. The modes then continue to wander relatively independent of the injection, until the mode closest to the injection frequency momentarily locks again to the injection laser, and initiates a new burst upon release from the locked state. We can thus conclude from these results that the bursting dynamics is due to strong, intermittent interactions of the injected beam with the longitudinal mode closest to the injection frequency, which gives rise to brief periods of locking followed by intensity bursts upon release from the locked state.

In spite of the apparent similarity between the behaviors of the free-running laser and the injected laser between bursts, a close comparison of Figs. 3(b) and 4(b) reveals that the modes of the injected fiber laser are never completely free of the influence of the injected light field. Indeed, Fig. 4(b) shows that the intensity of the longitudinal mode closest to the injection frequency (as measured from its gray level) is significantly higher than that of its neighboring modes, whereas in the absence of injection [Fig. 3(b)] the power is nearly equally distributed among all the modes represented. Thus, there is always a confinement of the optical spectrum of the injected laser around the injection frequency.

The analysis presented so far refers to the situation where the injected frequency is tuned to resonance with respect to the peak of the fiber laser output spectrum. However, we noted in the preceding section that bursting occurs over a wide range of injection wavelengths. The considerations made in the previous paragraphs help us to explain this fact: given the close spacing of longitudinal modes and the broadness of the gain line of the fiber laser, even injection wavelengths far away from the gain peak of the laser will have a longitudinal mode close enough (always within 5 MHz) to interact with, generating bursting dynamics. Certainly, the intensity of the bursting will decrease with injection detuning, until the gain of the closest longitudinal mode is not enough to induce the bursts (which in our case occurs for a wavelength detuning of ~ 14 nm).

The heterodyne measurement described in this section has given us some insight into the origin of the bursting dynamics, in terms of the frequency interaction and locking between the fiber laser modes and the injected field. However, it would be desirable to have a more quantitative description of this interaction. By way of example, the width of the injection locking range of our laser can be expected to determine how close to the reference frequency a given longitudinal mode of the laser must be in order to lock to the injected signal. In order to provide a quantitative answer to this and other questions, we develop in what follows a rate-equation model that exhibits the observed bursting behavior.

IV. A PHENOMENOLOGICAL RATE-EQUATION MODEL

Guided by the results presented in the preceding section, we restrict ourselves to analyzing the interaction between the (stationary) coherent injection field and the (dynamically evolving) longitudinal mode of the fiber laser closest to the injection frequency. Since we are only interested in describing the dynamics of one of the lasing modes of the laser, we consider the following single-mode rate-equation model:

$$\frac{dE}{dt} = (G-\alpha)E - i\Delta\omega E + E_{\mathrm{inj}} + \eta(t),$$

$$\frac{dG}{dt} = \frac{1}{T}(p - G - G|E|^2), \tag{1}$$

where $E(t)$ is the slowly varying complex amplitude of the relevant cavity mode and $G(t)$ represents the gain of the medium. The equations are written in a reference frame rotating at the injection frequency ω_{inj}, so that $\Delta\omega$ represents the detuning between the cavity mode frequency and the reference frequency. Measuring time in terms of the cavity round-trip time τ_c, the dimensionless detuning takes the form $\Delta\omega = (\omega_{\mathrm{inj}} - \omega_c)\tau_c$. Other parameters of this model are the cavity loss coefficient α, the amplitude of the intracavity injected field E_{inj}, and the pump rate p. The coefficient $T = \tau_f/\tau_c$ is the ratio between the fluorescence lifetime τ_f and the cavity round-trip time. The threshold pump rate for lasing action is $p_{\mathrm{thr}} = \alpha$. Finally, $\eta(t)$ is a Gaussian white noise of zero mean and intensity D_{sp} representing spontaneous emission fluctuations.

Rate-equation models have been used in the past to describe diverse properties of fiber lasers [27–30]. However, these models provide an extremely simplified description of these lasers. In the particular case of model (1), we are using a single linearly polarized field to represent the dynamics of a laser with a very large number of longitudinal modes, and no well-defined polarization. For this reason, there are few parameters of the model which we can directly identify with their corresponding experimental values for our laser: only the fluorescence lifetime $\tau_f = 10$ ms and the cavity round trip time $\tau_c = L/(c/n) = 200$ ns. The rest of the parameters will be fit to reproduce the experimentally observed dynamics.

We will see that, in spite of the simplifications made, this elementary model reproduces our experimental observations in a very satisfactory way.

In order to determine the values of the pump rate p and cavity loss coefficient α of our model, we fit the model to reproduce the experimentally measured relaxation oscillation frequency ($\nu_{\mathrm{RO}} \sim 45$ kHz) and their damping time ($T_{\mathrm{damp}} \sim 0.2$ ms). Linear stability analysis of the stable lasing solution of Eq. (1) in the absence of injection gives the following expressions for those two quantities:

$$\nu_{\mathrm{RO}} = \frac{1}{2\pi\tau_c}\sqrt{\frac{2(p-\alpha)}{T}}, \quad T_{\mathrm{damp}} = \frac{2T\alpha\tau_c}{p}. \tag{2}$$

Imposing the measured values of ν_{RO} and T_{damp} and with $T = 5\times10^4$, one obtains that $\alpha = 0.8$ and $p = 80$. We note that the required pump is much higher than the experimental value. This could be due to the fact that the mean-field approximation inherent to the rate equation model (1) underestimates the gain of the laser, requiring a larger pumping than the actual one.

Typical values of the injected power used in the experimental study described above correspond to injected amplitudes in the model on the order of $E_{\mathrm{inj}} = 0.1$. The width of the locking range for that injected amplitude can be computed by determining the detuning interval for which the stationary locked state is stable [20]. In our case, the calculation gives a locking range of ± 0.01 MHz, much smaller than the experimentally observed range of the frequency wandering. Given the complexity of the bifurcation diagram that this kind of systems display close to the locking range (see, for instance, Ref. [18] for an example comparing successfully experimental and theoretical results), we can expect the frequency dynamics of the fiber laser to play a vital role in the behavior of the system, by taking the laser through all detuning ranges (see beginning of Sec. III). Keeping this in mind, we have modeled phenomenologically the frequency wandering (which we believe to be a multimode effect, and it is not exhibited by the simple single-mode rate equation model) by adding a fluctuating term to $\Delta\omega$ in the form of a Gaussian nonwhite noise $\xi(t)$, with zero mean and a temporal correlation in the form

$$\langle \xi(t)\xi(t') \rangle = \frac{D_\omega}{\tau_\omega} e^{-|t-t'|/\tau_\omega}, \tag{3}$$

where τ_ω is the correlation time of the noise and D_ω is its intensity. Then, the detuning term now has the form $\Delta\omega = \Delta\omega_0 + \xi(t)$, where $\Delta\omega_0 = \Delta\nu_0/(2\pi)$ is the baseline value around which the detuning fluctuates, and $\xi(t)$ is the Ornstein-Uhlenbeck noise defined above. All three parameters of the fluctuating detuning, τ_ω, D_ω, and $\Delta\nu_0$, should be basically independent of the injection amplitude, and only the mean detuning $\Delta\nu_0$ varies from experiment to experiment in an inherently random way. $\Delta\nu_0$ is restricted to values of the order of a few megahertz, since the model considers the cavity mode closest to the injected frequency, and there is always one within the free spectral range of the laser, which is 5 MHz. By systematically comparing simulations with the experimental observations of the free running laser, we have chosen $D_\omega = 2\times10^3$ and $\tau_\omega = 2\times10^3$ (corresponding to a correlation time of 0.4 ms). Figure 5 shows a comparison between experimental output intensity measurements and corresponding numerical time traces obtained from model (1), for three different injection levels. The main qualitative characteristics of the experimental irregular bursting behavior are clearly reproduced by the model.

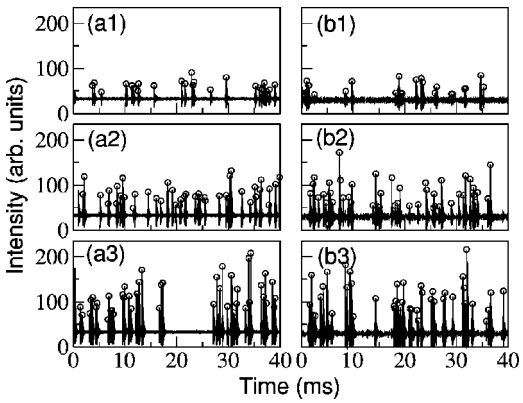

FIG. 5. Experimental (a) and numerical (b) time series exhibiting bursting dynamics, for three different injection levels. For the experimental traces, the injection ratio is 3.0×10^{-4} (a1), 7.6×10^{-4} (a2), and 1.9×10^{-3} (a3). For (b), $D_\omega = 2\times10^3$, $\tau_\omega = 2\times10^3$, $\Delta\nu_0 = 1$ MHz, and the injection ratio P_{inj}/P_L is 7.6×10^{-5} (b1), 2.3×10^{-4} (b2), and 1.4×10^{-3} (b3). The open circles indicate bursts that have been identified by our detection algorithm.

In order to examine the relationship between the frequency dynamics and the bursting events produced by the model described above, we compute the instantaneous lasing frequency as the time derivative of the phase of the complex envelope $E(t)$. Given that the reference frequency at which $E(t)$ rotates is the injection frequency, that quantity corresponds directly to the instantaneous detuning between the lasing and the injected frequencies, which is the measure obtained from the heterodyne experiments of Sec. III. Figure

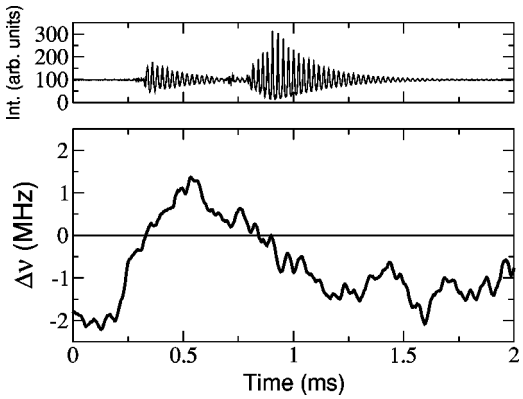

FIG. 6. Frequency evolution of the modeled fiber laser corresponding to two bursts. The frequency detuning $\Delta\nu$ is computed as the time derivative of the instantaneous phase of $E(t)$. Its time series has been filtered at 50 kHz in order to mimic the experimental bandwidth detection. The noise parameters are those of Fig. 5, with $P_{\mathrm{inj}}/P_L = 10^{-4}$.

6 shows a comparison between an intensity time series exhibiting two bursts and the corresponding frequency evolution. The horizontal line corresponds to resonance between the fiber laser and injection frequencies. We note that the estimated locking range (± 0.01 MHz) is too small to be discernible in the vertical detuning axis of the figure. Keeping this in mind, we observe that the bursts occur whenever the lasing frequency gets close enough to the locking range. The time the laser is actually locked is too small to be distinguished in this case (the same thing is expected to happen in the experiment for injection powers smaller than that considered in Fig. 4). As in the experimental results of Fig. 4, the bursts are followed by relaxation oscillations of the laser towards the unlocked state. Hence, on the basis of the modeling results we can interpret the bursting phenomena as due to the fact that close to the locking range boundaries strong dynamical behavior arises [19], which momentarily perturbs the laser and induces bursting.

V. STATISTICAL ANALYSIS OF THE BURSTING EVENTS

As we have seen above, the phenomenological model introduced in the preceding section reproduces satisfactorily the qualitative features of the bursting dynamics exhibited by our injected fiber laser. In order to undertake a more quantitative comparison, we now perform a statistical analysis of the bursting events, both for the experimental and numerical observations. Obtaining an agreement between these two types of results is in principle nontrivial, given that the noise-driven character of the numerical bursts could be expected to lead to statistical properties very different from those of the experimental bursts. In what follows, we will see that this is not the case, and that the agreement indeed exists, reinforcing the value of the model used and the conclusions drawn from it.

Both the experimental and numerical bursts can be identified by analyzing the corresponding time series. In the two cases, the series of relaxation oscillation maxima are detected, and the relative maxima of this series are taken to correspond to bursts, provided their intensity surpasses a certain threshold (which eliminates spurious results corresponding to the strongly fluctuating ''steady'' interburst phases). The threshold is taken to depend linearly on the standard deviation of the time series, which allows a direct comparison of different injection levels (for which the burst amplitudes, and thus the standard deviation of the time series, vary, as can be seen in Fig. 5). The results of this detection algorithm are plotted as empty circles in Fig. 5.

A first straightforward measure of the bursting distribution is the average of the time interval τ between consecutive bursts. After detecting the bursts by the technique described in the preceding paragraph, we compute their mean time separation for increasing levels of injection, for both the experimental and the numerical case. The results are compared in Fig. 7, which shows that the mean interburst interval slowly decreases with the injection level in the two sets of data. This behavior can be understood in the light of the injection model used: given that the detuning interval for which injection locking exists increases linearly (at least for small detunings) with the injection amplitude [20], an increase in the injection level will also lead to an increased probability that the wandering frequency hits the locking region and thus produces bursting.

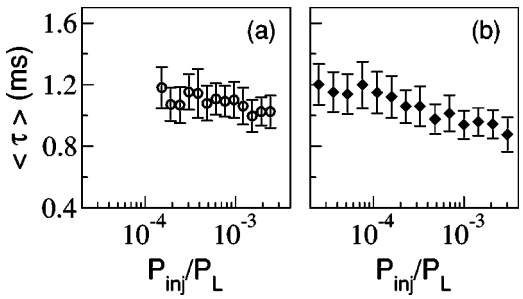

FIG. 7. Average time separation between consecutive bursts for increasing injection levels, for both experiments [(a) empty circles] and model [(b) full diamonds]. In the latter case, parameters are those of Fig. 5.

In contrast to other bursting phenomena encountered in nature [2,6,8], the bursts exhibited by our injected fiber laser are strongly aperiodic, both in terms of their amplitudes and their time separation. In order to establish any regularity that might exist in those quantities, in spite of their seeming complexity, we compute the probability distribution functions of the burst amplitudes I_m and interburst time separations τ. The computed probability distribution functions for the two quantities are plotted in log-log scale in Figs. 8 and 9, both for the experimental and the numerical data. In all cases, results for three different injection powers are plotted.

Figure 8 shows that the probability distribution functions of the interburst time intervals exhibit a clear power-law decay extending over more than one decade, with the same characteristic exponent independent of the injection level. The agreement between experimental and numerical data is remarkable. The exponent in the two cases is of the order of -1.45. Similar scaling laws have been obtained previously in on-off intermittency in noise-driven systems, such as electroconvection in liquid crystals [31].

Figure 9 displays the probability distribution functions of the burst amplitudes, again for both experiments (left plots)

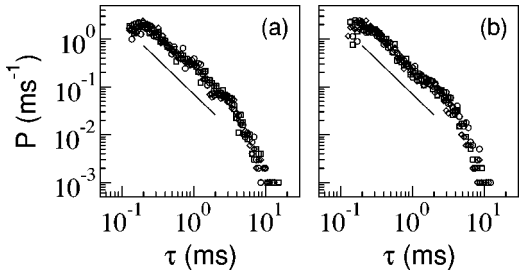

FIG. 8. Probability distribution function of the interburst time intervals for the experimental (a) and numerical (b) data. Three different injection levels are plotted in each case. For the experiments the injection/lasing power ratios are: 3.8×10^{-4} (circles), 9.6×10^{-4} (squares), and 2.4×10^{-3} (diamonds). For the numerics, the values of the injected amplitude E_{inj} are: 8.1×10^{-5} (circles), 2.3×10^{-4} (squares), and 1.4×10^{-3} (diamonds). Lines correspond to a power law decay with exponent -1.45.

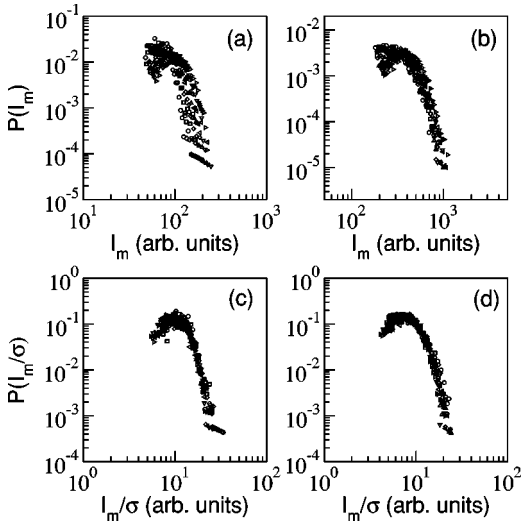

FIG. 9. Probability distribution function of the burst amplitudes for the experimental (a), (c) and numerical (b), (d) data, and different injected power ratios corresponding to the last seven points in each of the plots of Fig. 7. In plots (c) and (d) the data have been scaled by the standard deviation of the total intensity time series.

and simulations (right plots). As shown in the bottom row, when the graphs are scaled by the standard deviation of the corresponding intensity time series, all data collapse to the same function. The behavior is similar for both the experimental and numerical results. A region of power-law behavior can also be distinguished for large amplitudes in the two cases. These results also agree, at least qualitatively, with observations in systems exhibiting on-off intermittency.

In spite of the very good agreement observed so far between model and experiments, certain differences can be found in the response of the system to injection. The discrepancies are shown in Fig. 10, which presents the dependence of the standard deviation of the time series with the injected power ratio. In the experimental case [Fig. 10(a)] the resulting relation is seen to be a power law for all injections tested in the experiment, with a growth exponent close to 0.5. In the numerical case [Fig. 10(b)], however, a crossover is seen at $P_{\mathrm{inj}}/P_L \approx 3\times 10^{-4}$ between two different exponents, from a value close to 0.45 for low injections to ~ 0.2 for large injection powers.

VI. CONCLUSIONS

We have shown experimentally that small levels of near resonant light injection applied to an erbium-doped fiber ring laser give rise to intense bursts in the light emitted by the laser, occurring at irregular times and with irregular amplitudes. Heterodyne measurements show that the fiber laser undergoes a slow frequency wandering in the absence of injection. In the presence of injection, the bursting is associated with a momentary locking of the laser to the injected signal, followed by an abrupt escape from the locking region, which gives rise to the bursts. A numerical analysis of a rate-equation model, where the frequency wandering is introduced phenomenologically by means of an Ornstein-Uhlenbeck noise, confirms that the locking range of the system is very small in comparison to the range of the frequency wandering, and shows that the bursts occur when the laser frequency gets close enough to the locking range. Even though the bursting events are noise driven, a statistical study of their time separation and amplitude reveals a power-law decay of the corresponding probability distribution function, characteristic of on-off intermittency. The good agreement between the statistical analyses of experimental and numerical data indicates that the heuristic modeling of the frequency wandering in terms of a time correlated noise is very adequate. The cause of this wandering, and its possible relationship with the strongly multimode character of fiber lasers, is under current investigation.

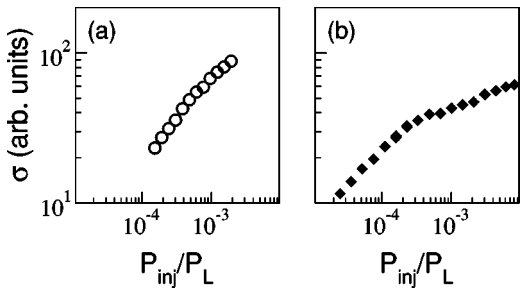

FIG. 10. Standard deviation of the total intensity time series vs the injected power ratio, for both the experimental (a) and numerical (b) data.

ACKNOWLEDGMENTS

We thank B. Krauskopf and V. Kovanis for fruitful discussions. D.J.D. and R.R. thank Brian Tighe for his contributions in the initial stages of the experimental observations. Financial support from the Office of Naval Research is acknowledged. J.G.O. also acknowledges support from DGES (Spain, Project Nos. BFM2001-2159 and BFM2002-04369) and from the Generalitat de Catalunya (Project No. 2001SGR00223 and Travel Grant No. 2001BEAI400104).

[1] K. Coughlin and P.S. Marcus, Phys. Rev. Lett. **77**, 2214 (1996).
[2] J. Moehlis and E. Knobloch, Phys. Rev. Lett. **80**, 5329 (1998).
[3] D. Sweet, E. Ott, T.M. Antonsen, and D.P. Lathrop, Phys. Plasmas **8**, 1944 (2001).
[4] M.A. Malkov, P.H. Diamond, and M.N. Rosenbluth, Phys. Plasmas **8**, 5073 (2001).
[5] P.M. Woods, C. Kouveliotou, J. van Paradus, T.M. Koshut, M.H. Finger, M.S. Briggs, G.J. Fishman, and W.H.G. Lewin, Astrophys. J. **540**, 1062 (2000).
[6] J. Keener and J. Snyder, *Mathematical Physiology* (Springer, New York, 1998).
[7] C.O. Weiss and R. Vilaseca, *Dynamics of Lasers* (VCH, Weinheim, 1991).

[8] R. Meucci, A. Di Garbo, E. Allaria, and F.T. Arecchi, Phys. Rev. Lett. **88**, 144101 (2002).
[9] R. Lang, IEEE J. Quantum Electron. **18**, 976 (1982).
[10] D.J.W. Brown, C.G. Whyte, D.R. Jones, and C.E. Little, Opt. Commun. **137**, 158 (1997).
[11] W.H. Chung, L.Y. Chan, H.Y. Tam, P.K. Wai, and A.S. Demokan, IEEE Photonics Technol. Lett. **14**, 920 (2002).
[12] C.O. Weiss, E. Bava, A. DeMarchi, and A. Godone, IEEE J. Quantum Electron. **16**, 498 (1980).
[13] D.G. Slavov and M.N. Nenchev, Opt. Commun. **200**, 283 (2001).
[14] T. Pawletko, M. Houssin, M. Knoop, M. Vedel, and F. Vedel, Opt. Commun. **174**, 223 (2000).
[15] Y. Liu, H. K. Liu, and Y. Braiman, Appl. Opt. **41**, 5036 (2002).
[16] J.R. Tredicce, F.T. Arecchi, G.L. Lippi, and G.P. Puccioni, J. Opt. Soc. Am. B **2**, 173 (1985).
[17] A. Gavrielides, V. Kovanis, and T. Erneux, Opt. Commun. **136**, 253 (1997).
[18] S. Wieczorek, T.B. Simpson, B. Krauskopf, and D. Lenstra, Phys. Rev. E **65**, 045207 (2002).
[19] B. Krauskopf and S. Wieczorek, Physica D **173**, 114 (2002).
[20] E.G. Lariontsev, I. Zolotoverkh, P. Besnard, and G.M. Stéphan, Eur. Phys. J. D **5**, 107 (1999).
[21] M.K.S. Yeung and S.H. Strogatz, Phys. Rev. E **58**, 4421 (1998).
[22] G.P. Agrawal, *Fiber-Optic Communication Systems* (Wiley, New York, 1992).
[23] P.K. Cheo, A. Liu, and G.G. King, IEEE Photonics Technol. Lett. **13**, 439 (2001).
[24] G.D. VanWiggeren and R. Roy, Science **279**, 1198 (1998); G.D. VanWiggeren and R. Roy, Phys. Rev. Lett. **81**, 3547 (1998).
[25] E. Desurvire, *Erbium-Doped Fiber Amplifiers—Principles and Applications* (Wiley, New York, 1994).
[26] I. McMackin, C. Radzewicz, M. Beck, and M.G. Raymer, Phys. Rev. A **38**, 820 (1988).
[27] S.A. Zenchenko, S.V. Leshkevich, A.I. Portnyagin, S.P. Puchek, and A.E. Filippov, Kvant. Elektron. (Moscow) **17**, 841 (1990) [Sov. J. Quantum Electron. **20**, 760 (1990)].
[28] M. Le Flohic, P.-L. Francois, J.-Y. Allain, F. Sanchez, and G.M. Stéphan, IEEE J. Quantum Electron. **27**, 1910 (1991).
[29] S. Bielawski, D. Derozier, and P. Glorieux, Phys. Rev. A **46**, 2811 (1992).
[30] E. Lacot, F. Stoeckel, and M. Chenevier, Phys. Rev. A **49**, 3997 (1994).
[31] T. John, U. Behn, and R. Stannarius, Phys. Rev. E **65**, 046229 (2002).